RESEARCH ARTICLE

ADVANCED
INTELLIGENT
SYSTEMS
Open Access

www.advintellsyst.com

Amplitude-Controlled Electromagnetic Pulse Switching Using Waveguide Junctions for High-Speed Computing Processes

Ross Glyn MacDonald, Alex Yakovlev, and Victor Pacheco-Peña*

Performing computational tasks with wave-based devices is becoming a groundbreaking paradigm that can open new opportunities for the next generation of efficient analogue/digital computing systems. Decision-making process for switching and routing of signals is fundamental for computing as it enables the transfer of information from one to many (or single) blocks within a system. Herein, a technique is proposed for the design of pulse-based switching devices for the computing of fundamental decision-making processes. Information is encoded from multiple channels as transverse electromagnetic (TEM) pulses of varying amplitudes and polarities propagating through interconnected parallel plate waveguides modeled as simple transmission lines. An in-depth description of the technique is presented showing how switching and routing of information can be engineered by exploiting the linear splitting and superposition of multiple pulses traveling through waveguide junctions. To demonstrate the potential of the technique, two devices are developed: a *comparator* which can calculate the largest value between two real-valued numbers and a *pulse director* which exploits the reciprocity of waveguide junctions to create a similar yet different performance of a traditional AND gate (emulating its performance via the analogue linear system). These findings may open new pathways for high-speed electromagnetic pulse-based computing systems.

1. Introduction

In his 1965 paper,[1] Gordon Moore described the relationship between the density of transistors on a silicon chip and the operational speed of that chip. In this seminal work, which is now known as Moore's law, he envisioned that the density of these devices would double every 18 months. In the years since its publication, this prediction has been found to be remarkably accurate.[2] This rapid advancement has been possible by the tremendous scalability of semiconductor devices such as metal–oxide–semiconductor field-effect transistors (MOS-FETs).[3,4] However, Moore recognized that this fast rate of advancement would someday become difficult to continue as there are limits to how small transistor-based devices can be made,[5,6] limits that many academics believe we are now reaching.[7,8] The ability to control the flow of energy via switching techniques can be considered as a fundamental process by which computation takes place. For instance, in classical computing devices, the flow of current is controlled by such semiconductor-based devices (transistors) working as switching elements. However, intrinsic parasitic capacitances are difficult to avoid in such devices. These unwanted reactive elements are charged and discharged during the dynamic switching process performed by transistors, adding further delays to the overall computations which restrict the speed and efficiency of the devices.[9]

To overcome this, new paradigms on computing are needed. Different scenarios have been recently proposed such as spintronics,[10] biological computing,[11] computing with electromagnetic (EM) waves,[12,13] and optical solitons,[14–18] among others. EM wave-based computing has become a hot research topic worldwide as the information can be transferred at the speed of light in the medium where the wave propagates. In this context, such fully EM wave-based computing systems that do not require charging/discharging processes have the potential to open new avenues for future high-speed computing.[6]

In this realm, metamaterials (MTMs) and metasurfaces (MTSs), as their 2D version, have been recently applied to the field of computing using EM waves.[19–21] MTMs are artificial materials that exhibit EM responses not always easy to find in natural media such as negative or near-zero permittivity values.[22–24] MTMs have successfully been applied in multiple scenarios such as sensing,[25,26] antennas,[27,28] and imaging,[29,30] demonstrating their ability to arbitrarily control fields

R. G. MacDonald, V. Pacheco-Peña
School of Mathematics, Statistics and Physics
Newcastle University
Newcastle Upon Tyne NE1 7RU, UK
E-mail: victor.pacheco-pena@newcastle.ac.uk

R. G. MacDonald, A. Yakovlev
School of Engineering
Newcastle University
Newcastle Upon Tyne NE1 7RU, UK

and waves not only in space but also in time.[22,31–37] This arbitrary manipulation of fields and waves allowed by MTMs has recently been exploited and applied to analogue computing where useful operations such as differentiation, integration, and convolution have been demonstrated using waves instead of electrical signals.[38–44] This has inspired the scientific community to propose further approaches for alternative computing using EM waves with outstanding examples including optical quantum computing[45,46] and resonant plasmonic flow networks.[47–50] As with electrical signals in classical computing circuits, switching EM waves is a key process that can be exploited to emulate optical logic operations. Recent examples in this area include the demonstration of logic gates using plasmonic waveguides,[51–55] graphene cylindrical resonators,[56] and solitons traveling along long chain of polymers,[57,58] to name a few. In this realm, we have also recently shown a method for EM pulse switching based on interconnected waveguides in series and/or parallel configurations.[59,60] We have shown how transverse electromagnetic (TEM) pulses of equal amplitude interacting within such structures can constructively/destructively interfere producing new TEM pulses which will or will not propagate down each of the connected waveguides, a response that depends on the polarities (positive or negative) of the TEM pulses used as excitation signals[59,61,62] (i.e., this is a passive system based on linear interferometry[51–53,56,63]).

Inspired by the importance of waves for future computing systems and the need of switching elements as the basis for complex computing processes, in this work we build upon our recently proposed technique to demonstrate a method for high-speed amplitude-controlled switching of EM pulses in multiple waveguide-based junctions. We want to push the boundaries of EM pulse switching by considering junctions being excited by multiple ports at the same time using TEM pulses with different polarities and amplitudes. The underlying physics of the proposed structures are discussed in detail via the scattering matrix approach.[61,64] We provide an in-depth analytical study for the transmission and reflection of pulses between waveguides being connected in series or in parallel. We exploit this technique to demonstrate how these simple, yet interesting waveguide-based junctions can be used to create amplitude-controlled EM pulse switching devices by considering the interaction of pulses in a three-waveguide system. It is shown how it can be implemented for the design of comparators which can switch between two states based on the relationship between two inputs. For instance, we discuss how such three-waveguide configurations can be used to compare two numbers (φ_1 and φ_2) being mapped as the amplitude of the TEM pulses excited from two different waveguides. It will be shown how the proposed comparator can generate a pulse (traveling toward the third waveguide) with either a negative or a positive polarity when $\varphi_1 < \varphi_2$ and $\varphi_1 > \varphi_2$, respectively. We further unleash the potential of our amplitude-based switching approach for the design of an EM pulse directing device with the ability to redirect all the pulses in the system (being excited from all the waveguides at the same time) down to a single waveguide, with zero reflection toward the rest of the waveguides. A full physical description of such directing device is presented demonstrating how a "matched condition" for the amplitude and polarities of all input pulses should be fulfilled, a condition that also depends on the number of

waveguides present in the system. We also provide examples using N-interconnected waveguides for completeness. All analytical results in this study are corroborated by numerical simulations using the transient solver of the commercial software CST Studio Suite, demonstrating an excellent agreement with the theoretical values. In practice, these structures could be excited with known microwaves techniques and circuit methods such as line drivers and buffers on transmission lines and using vector network analyzers.[65–67] Our technique for amplitude-based switching of TEM pulses could be exploited in scenarios where decision-making processes are needed such as in the emulation of Boolean logic via analogue linear systems and signal processing tasks.

2. Results

2.1. Analytical Formulation of the Proposed Technique

In our proposed technique, decision-making processes are performed based on the interaction between TEM square pulses at waveguide crossings (or junctions). The polarity (+ or −) of the transmitted/reflected pulses seen at the waveguide ports can be manipulated by correctly controlling the amplitude of the TEM pulses excited at the ports. As it will be shown, this will enable us to emulate elementary If … Then … Else operations which are fundamental decision-making processes in computing.[68]

To begin with, let us first consider the interaction of TEM square pulses within a network using interconnected 2D parallel plate waveguides (see **Figure 1**). As in ref. [59], we consider two types of junctions by using 2D waveguides connected either in parallel or series (see Figure 1a,b, respectively). Such interconnected waveguides can be represented as transmission lines (TLs)[61] and their equivalent model is shown at the bottom of each network in Figure 1a,b. In this realm, known TL techniques[61,64] can be exploited to represent the interaction of TEM square pulses when being excited from different ports inside the network. In our approach we consider TEM square pulses of amplitude $A \in \mathbb{R}$ with its sign representing either a positive (+) or negative (−) polarity. Following ref. [59], the polarity of the pulses is mapped by drawing an arrow parallel to a TEM square pulse starting at the base (zero-value) voltage and then directed toward the nonzero voltage (see Figure 1c). For parallel junctions, pulses with arrows directed toward the top/bottom metallic plate are defined as pulses with a +/− polarity, respectively. For junctions in series, TEM square pulses with arrows directed clockwise/anticlockwise around the junction are mapped as +/− polarity.[59]

For N-interconnected TLs (as shown in Figure 1), we can represent the input and output TEM pulses in the network by defining two vectors, namely, $\mathbf{x} = [x_1, x_2,..., x_N]$ and $\mathbf{y} = [y_1, y_2,..., y_N]^T$, respectively, with subscripts 1, 2...N representing each waveguide in the network and T as the transpose operator. In this context, each x_i and y_i element represents the amplitude of the TEM square pulses as described above. The analytical formulation of the N-interconnected TLs was recently shown in ref. [59] but we explain its fundamental principles here for completeness noting that this will be further exploited below for decision-making processes using TEM pulses with nonequal
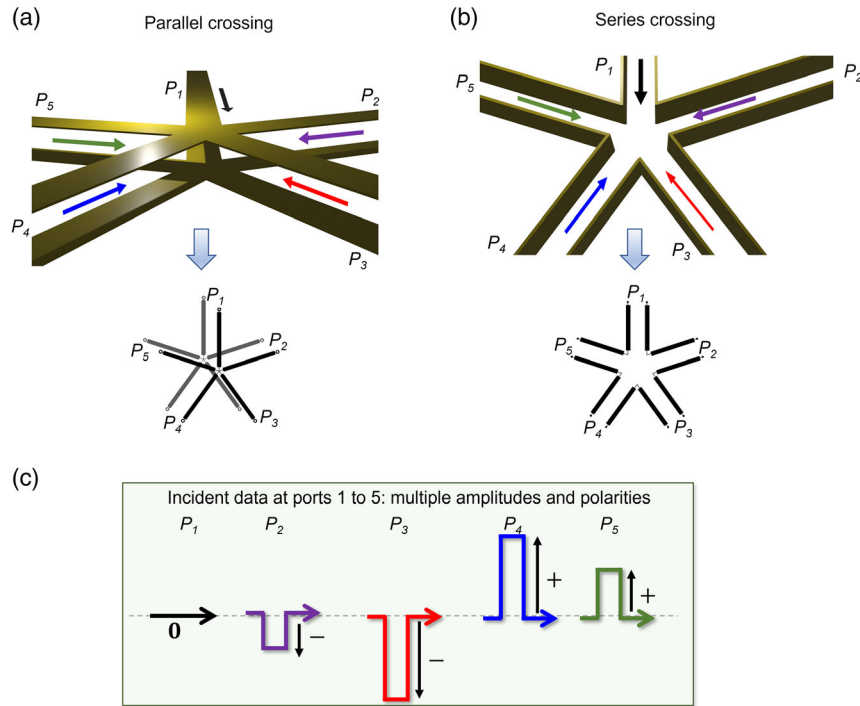
ADVANCED
SCIENCE NEWS
www.advancedsciencenews.com

ADVANCED
INTELLIGENT
SYSTEMS
Open Access

www.advintellsyst.com

Figure 1. Schematic representation of parallel and series waveguide junctions. a,b) 3D render of five-input 2D parallel plate waveguide junctions in parallel and series configurations, respectively. The equivalent transmission line representation of each waveguide junction is shown at the bottom of each panel for completeness. Here, the lower/upper set of metallic plates are represented by gray/black cylinders in the transmission line model, respectively, to guide the eye. c) Examples of different potential input signals which may be excited at each of the waveguide ports labeled as P_1–P_5.

amplitudes and polarities. Assuming that all incident TEM square pulses have the same temporal duration and that they arrive at the junction simultaneously (note that we consider that all the wavelengths/TLs are filled with the same materials, air in our case $n_0 = 1$), the vectors γ and x can be related by the scattering matrix of the junction, A.[59]

$$\gamma = Ax^{\mathrm{T}} \tag{1}$$

It is important to highlight that A will generally depend on the geometry and material composition of the waveguides present at the junction. However, when all waveguides are identical, as their impedances are the same, the resulting matrix A can simply be expressed in terms of N (see the full derivation in the Section S1, Supporting Information). In this context, $A = I - \gamma J$ and $A = -I + \gamma J$ for series and parallel junctions, respectively, where I and J are the identity and all-ones matrices of size $N \times N$, respectively, and $\gamma = 2/N$ is the transmission coefficient which depends on the number of waveguides at the junction, as expected. As an example, we can follow this approach to calculate the output vector γ of a parallel junction using three-interconnected waveguides, resulting in

$$\gamma = \begin{pmatrix} \frac{-1}{3} & \frac{2}{3} & \frac{2}{3} \\ \frac{2}{3} & \frac{-1}{3} & \frac{2}{3} \\ \frac{2}{3} & \frac{2}{3} & \frac{-1}{3} \end{pmatrix} \begin{pmatrix} x_1 \\ x_2 \\ x_3 \end{pmatrix} = \begin{pmatrix} \frac{-1}{3}x_1 + \frac{2}{3}(x_2 + x_3) \\ \frac{-1}{3}x_2 + \frac{2}{3}(x_1 + x_3) \\ \frac{-1}{3}x_3 + \frac{2}{3}(x_1 + x_2) \end{pmatrix} \tag{2}$$

To better understand the implications of Equation (2), let us consider an example of such a parallel junction using three

waveguides being excited by two single pulses from two different ports simultaneously. This scenario is depicted in **Figure 2** where the amplitudes of the incident pulses are A and B considering a TEM pulse applied from P_1 or P_2, respectively (here we focus our attention on parallel junctions; the case using series junctions is also included in the Figure S1, Supporting Information, for completeness). A schematic representation of this configuration for a time t before and after the pulses have reached the crossing region is shown in Figure 2a,b, respectively. As observed, the interaction between the two pulses results in six TEM square pulses being re-emitted from the junction (three pulses created by each incident TEM square pulse). Pulses which are excited in the same waveguide interact via superposition, resulting into a single output TEM pulse traveling toward each of the ports (P_1 to P_3). Note that this interaction can be either constructive or destructive depending on the polarities of the re-emitted pulses: TEM pulses of opposite polarity will destructively interfere, producing a TEM pulse with lower or even almost zero amplitude. On the other hand, pulses of the same polarity will constructively interact resulting in a single pulse of increased amplitude. This response can be analytically verified by using Equation (1) with $x = [A, B, 0]$, as follows

$$\gamma = \begin{pmatrix} \frac{-1}{3} & \frac{2}{3} & \frac{2}{3} \\ \frac{2}{3} & \frac{-1}{3} & \frac{2}{3} \\ \frac{2}{3} & \frac{2}{3} & \frac{-1}{3} \end{pmatrix} \begin{pmatrix} A \\ B \\ 0 \end{pmatrix} = \begin{pmatrix} \frac{-1}{3}A + \frac{2}{3}B \\ \frac{-1}{3}B + \frac{2}{3}A \\ \frac{2}{3}(A + B) \end{pmatrix} \tag{3}$$
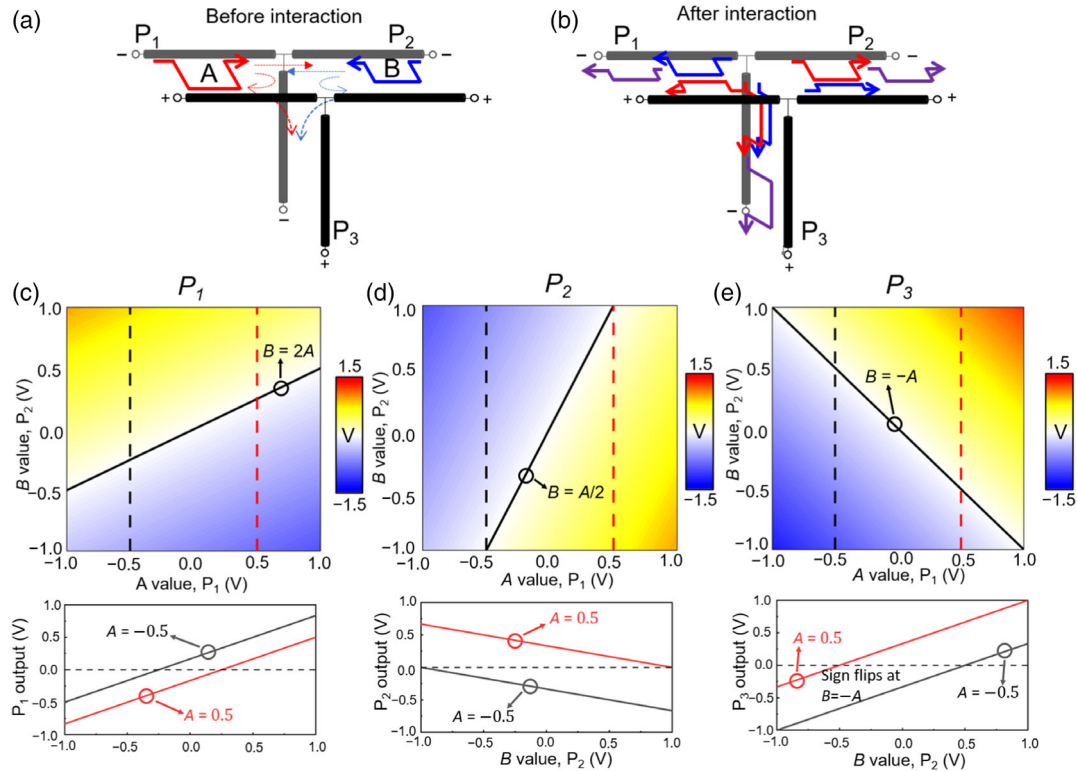
Figure 2. Two pulse interaction in a parallel junction formed by three interconnected parallel plate waveguides. a,b) Diagrams representing the interaction of the pulses at times before and after the incident pulses pass the crossing region. Two pulses of arbitrary amplitude are excited from P_1 and P_2; the splitting of each pulse is represented by arrows in (a). The individual pulses after splitting are shown in (b) (red and blue pulses) along with the resulting pulse after superposition (purple pulses). Waveguides are labeled as $+$ and $-$ to help the reader determine the polarity of the pulses at the waveguide port. If the voltage arrow (as shown in Figure 1c) points toward the waveguide labeled $+$ then the pulse has positive polarity and vice versa for an arrow pointing toward the waveguide labeled with $-$. As in Figure 1 gray/black cylinders in the transmission line models represent the lower/upper set of metallic plates for the waveguides, respectively. c–e) 2D plots representing the amplitude of the final output pulse observed at P_1, P_2, and P_3, respectively, as a function of the amplitudes A and B of the incident TEM pulses applied from P_1 and P_2, respectively. The bottom panels in c–e) represent the output pulse amplitude seen at P_1–P_3 extracted from the black and red dashed lines in c–e).

As an example, the full range of reachable output pulse amplitudes seen at P_1, P_2, and P_3 when A and B vary in the range $[-1,1]$ volts is presented in Figure 2c–e, respectively. To better compare these results, we extracted the amplitude of the detected pulses at each output port along the vertical dashed lines from Figure 2c,e and the results are shown at the bottom of each panel. As observed, the resulting pulses traveling toward P_1, P_2, and P_3 can be positive, negative, or even zero depending on the values of A and B. In this case, the inflection point between a positive or negative output pulse can be mathematically described by forcing an amplitude of 0 V for each of the ports from the right-hand side of Equation (3) resulting in $B = 2A$, $B = A/2$, and $B = -A$ for P_1, P_2, and P_3, respectively (to guide the eye, these expressions are also plotted as black solid lines in Figure 2c–e, respectively). Regarding the switching between distinguishable output states, the 0 V-lines are of particular importance as we can classify output states based on the polarity of the pulse (output is on one side of the 0 V-line or the other, i.e., positive or negative) or based on the existence, or lack thereof, a pulse (output is on the 0 V-line or not). Note that the condition $B = -A$ for P_3 (representing the bottom waveguide in Figure 2a,b as the waveguide without an incident TEM pulse) means that the TEM pulses from P_1 and

P_2 should be of opposite polarity but equal magnitude to achieve zero transmission toward P_3, an important feature that will be exploited in the following section to demonstrate a comparator as an example of a decision-making process using amplitude-controlled switching in N-interconnected waveguide junctions.

2.2. Comparator

In this section, we exploit three-interconnected waveguides in a parallel junction configuration, as shown in Figure 2a,b, to design a *comparator* as an example of a decision-making process. The purpose of this structure is to compare the values of two real numbers and to decide which one is larger/smaller. In our approach, each number is mapped as the amplitude of the TEM square pulses applied from either P_1 or P_2. The two numbers we wish to compare are labeled φ_1 and φ_2, respectively (φ_1, $\varphi_2 \in \mathbb{R}$). The comparator operation is realized by forcing destructive interference between the pulses scattered toward P_3 after the incident pulses (one from P_1 and one from P_2) have passed the crossing region. By observing Equation (3) such performance can be achieved if the incident pulses from P_1 and P_2

have opposite polarities, as expected. This is also shown in Figure 2e where the results of the output pulse at P_3 are shown along with the 0 V-line (which indicates complete destructive interference) plotted as black solid line. As it can be observed, the 0 V-line for P_3 has a negative slope (compared to the positive slope for the 0 V-lines of P_1–P_2, Figure 2c,d), indicating that destructive interference occurs when A and B have opposite polarity, as described above.

To design the *comparator*, we excite a TEM square pulse of amplitude $A = \varphi_1$ and $B = -\varphi_2$ from P_1 and P_2, respectively. With this configuration, the polarity of the pulse in P_1 will thus be the same as the sign of the number the pulse is representing (φ_1), while the polarity of the pulse in P_2 and the sign of the number (φ_2) are inverted. Following Equation (3), the amplitude of the output pulse toward P_3 can thus be written as

$$\gamma_3 = \frac{2}{3}(\varphi_1 - \varphi_2) \tag{4}$$

meaning that the polarity of the output pulse seen at P_3 will depend on the values of φ_1 and φ_2 such that if $\varphi_1 > \varphi_2$ the TEM pulse will have a positive polarity while it will be of negative polarity if $\varphi_1 < \varphi_2$. Finally, if $\varphi_1 == \varphi_2$, then no pulse will be observed at P_3 due to complete destructive interference of the two scattered pulses, as expected.[59] Note that as we exploit the polarity of the output pulse to classify the answer ($\varphi_1 > \varphi_2$ or $\varphi_1 < \varphi_2$), our linear system will only require that the values of φ_1 and φ_2 are different enough to produce an output pulse with an amplitude that falls within the dynamic range of a potential receiver/readout. Also, it is important to note that our pulse comparator is different than a digital comparator because in our case the inputs and the outputs can have different amplitudes which do not need to be classified as binary 1 or 0, i.e., we are dealing with an analogue system. In this context, it is the polarity ($+$ or $-$) not the amplitude of the output pulse what is the result of the decision-making process being carried out by the proposed pulse *comparator*. To verify our *comparator* using waveguide junctions (interconnected TLs) as a decision-making process, full-wave numerical simulations were carried out using the transient solver of the commercial software CST Studio Suite. TEM pulses with a duration of 0.4 ns were excited from P_1 and P_2. All the waveguides were considered to have the same dimensions (3 mm width and a separation between the metal plates of 3 mm) and vacuum was used as the filling material ($\varepsilon_r = 1$, $\mu_r = 1$). The length of the waveguides between each port and the junction is 250 mm. With this configuration, the TEM pulses propagate through the waveguides at the speed of light in vacuum (see more details of the numerical setup in the Experimental Section).

The numerical result of the out-of-plane electric field (E_y) distribution at different times along with the voltage of the ports as a function of time is shown in **Figure 3**. In both Figure 2b and 3a, a snapshot of the incident pulses at a time instant before ($t = 2.5$ ns) and after ($t = 3.4$ ns) they interact at the junction is shown in the top and bottom panels, respectively. For completeness, here we consider two possible cases: when $\varphi_1 < \varphi_2$ (case 1, Figure 3a) and when $\varphi_1 > \varphi_2$ (case 2, Figure 3b). Without loss of generality, in both cases shown in Figure 3 the smaller and larger numbers to be compared are chosen to

be 3 and 5, respectively (note that our approach also applies for negative values of φ_1 and φ_2, see Section S2, Supporting Information, for an example), resulting in the following incident pulses amplitudes: (case 1) 3 V at P_1, -5 V at P_2 and (case 2) 5 V at P_1 and -3 V at P_2. By observing the numerical results from Figure 3, the amplitude of the pulse traveling toward P_3 is -1.3379 and 1.3379 V when $\varphi_1 = 3 < \varphi_2 = 5$ (Figure 3a) and when $\varphi_1 = 5 > \varphi_2 = 3$ (Figure 3b), respectively. These results are in excellent agreement with the theoretical values predicted by Equation (4): $-(4/3)$V and $(4/3)$V in P_3 for the same two cases in Figure 3a,b, respectively. These results demonstrate how a *comparator* between two arbitrary real numbers can be designed by using our approach for TEM square pulse switching via waveguide junctions.

2.3. Pulse Director

In addition to the *comparator* presented in the previous section as an example of a decision-making process, in this section we will consider an additional device in which all input TEM square pulses are redirected toward a single waveguide with no TEM pulses being reflected to any other waveguide, a structure that we call a *pulse director*. As it will be shown later, such pulse director can be generalized to a N-waveguide junction. However, we will initially consider the parallel junction with three waveguides as in the previous section. To find the conditions required for complete pulse redirection toward a single output waveguide, we exploit the reciprocity features of the scattering matrix shown in Equation (1). In this context, any output pulse vector γ may be used to reconstruct an input vector x by simply using γ as an input vector[59] (i.e., $x' = \gamma$). For example, let us consider the output vector $\gamma = [0,0,1]$V. To find the input vector required to construct this output, we can apply the scattering matrix from Equation (1) to the vector γ with $x' = \gamma$, as follows

$$x = \gamma' = \begin{pmatrix} \frac{-1}{3} & \frac{2}{3} & \frac{2}{3} \\ \frac{2}{3} & \frac{-1}{3} & \frac{2}{3} \\ \frac{2}{3} & \frac{2}{3} & \frac{-1}{3} \end{pmatrix} \begin{pmatrix} 0 \\ 0 \\ 1 \end{pmatrix} = \begin{pmatrix} \frac{2}{3} \\ \frac{2}{3} \\ \frac{-1}{3} \end{pmatrix} \tag{5}$$

meaning that the input TEM pulses excited in P_1 to P_3 should have an amplitude of $(2/3)$V, $(2/3)$V and $-(1/3)$V, respectively, to redirect all the pulses toward P_3 after they interact at the junction between the waveguides. Clearly, this vector $x = [2/3, 2/3, -1/3]$V is not the only solution to the redirection problem, as the choice of the amplitude of the input pulse for P_3 in Equation (5) was arbitrary. If the calculation in Equation (5) was repeated for the vector $\gamma = \zeta[0,0,1]$V, where ζ is some arbitrary constant $\in \mathbb{R}$, then $x = \zeta[2/3, 2/3, -1/3]$V. This means that any input vector that can be written in the form $x = \zeta[2/3, 2/3, -1/3]$V, for any real number ζ, will also result in a pulse redirection effect toward P_3. Examples include $x = [2,2,-1]$V and $x = [1/3, 1/3, -1/6]$V (i.e., $\zeta = 3$ and $\zeta = 1/2$, respectively), which results in the output vectors $\gamma = [0,0,3]$V and $\gamma = [0,0,1/2]$V, respectively. Here, the x vectors that satisfy this condition will be called *matched* input vectors, as the amplitudes and polarities of all input pulses are *matched* such that only transmission toward P_3 is allowed.
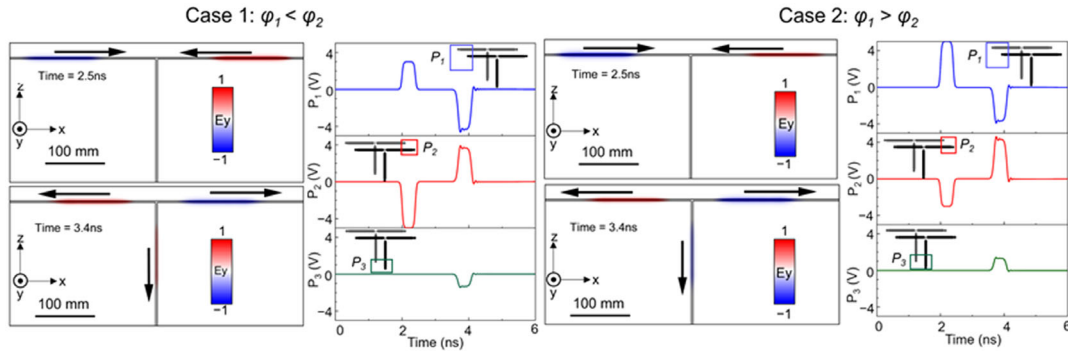
ADVANCED
SCIENCE NEWS
www.advancedsciencenews.com

ADVANCED
INTELLIGENT
SYSTEMS
Open Access

www.advintellsyst.com

Figure 3. Comparator operation, numerical results. a) Case 1, $\varphi_1 < \varphi_2$, considering TEM square pulses at P_1 and P_2 of are 3 and -5 V, respectively. b) Case 2, $\varphi_1 > \varphi_2$, considering TEM square pulses at P_1 and P_2 of are 5 and -3 V, respectively. The top-left and bottom-left panels of a) and b) represent the snapshot of the out-of-plane electric field distribution at a time $t = 2.5$ ns and $t = 3.4$ ns corresponding the times before and after the incident TEM square pulses from P_1 and P_2 have passed the crossing region, respectively). The line plots in the right panel show the voltage as a function of time for each port. All color scales for the out of plane electric field distributions are normalized to 950 V m^{-1}, corresponding to the maximum electric field obtained from the numerical results for an incident TEM pulse of 3 V pulse, which is close to the value expected considering an ideal waveguide with infinite plate size along the transversal xy plane (1000 V m^{-1}).

As described in the previous sections, after passing the crossing region, the incident TEM pulses applied from each port will create new TEM square pulses traveling in all the waveguides and the final signal that will be received in P_1–P_3 will be the result of the destructive/constructive interaction of the pulses inside each waveguide. This is illustrated in **Figure 4**a,b where we show a schematic representation of the division of each individual pulse in this system. Here, we show the case when the three-waveguide junction is excited with the *matched* input vector $x = [2,2,-1]$V as an example. After the pulses pass the junction (Figure 4b) each incident TEM pulse will generate a pulse traveling in each

waveguide toward P_1–P_3 with a voltage defined by Equation (2). However, as the matching condition for vector x is fulfilled, TEM pulses toward P_1 and P_2 eliminate between each other and only propagation toward P_3 is permitted. As shown in Figure 4b, all the pulses toward P_3 have the same polarity and thus are constructively added while in P_1 and P_2 the pulses completely destroy one another, as expected.

In Figure 4c and 5, we further explore the performance of the structure when the input vector x is chosen such that the *matched* condition is not achieved. Here, we consider the input vector $x = [A,B,C]$V where A, B, and $C \in \mathbb{R}$. Given that any *matched*
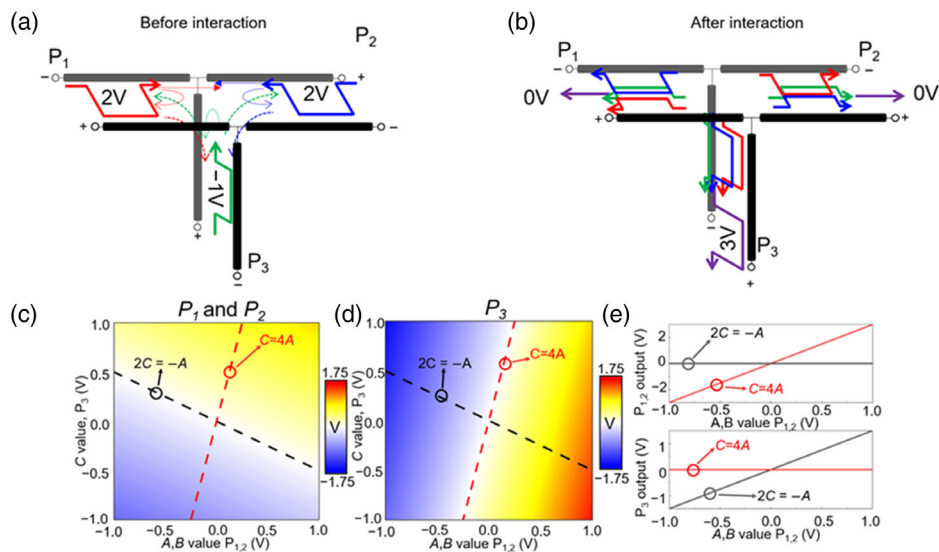

Figure 4. Three input pulse director operation. Pulse diagrams representing the splitting of individual pulses in the *matched* condition at a time instant a) before and b) after the pulses interact at the junction. Note that, as in Figure 2, the final pulses traveling toward the ports are the purple pulses. c,d) Analytical results of the voltage reachable for the output pulse for $P_1 = P_2$ and P_3, respectively, for the case when $A = B \in [-1,1]$V and $C \in [-1,1]$V. As in Figure 2, the labels $+$ and $-$ have been added to better observe the polarity of the pulses at the waveguide port. As in Figure 1, the upper/lower waveguides are represented by black/gray transmission lines, respectively. e) Output pulse amplitudes seen at $P_1 = P_2$ (top) and P_3 (bottom) when following the black and red dashed lines shown on the contour plots in c,d).

**ADVANCED
SCIENCE NEWS**

www.advancedsciencenews.com

**ADVANCED
INTELLIGENT
SYSTEMS**
Open Access

www.advintellsyst.com

input vector can be written as $\zeta[2, 2, -1]$ where ζ is a real constant, we can infer that for x to be *matched*, A must be equal to B. With this in mind, we first explore the range of output pulses seen at the waveguide ports when $A = B$ and C can vary in the range $[-1,1]$V. In this scenario, the output pulses seen at P_1 and P_2 are identical due to the symmetry of the system. With this setup, the amplitude of the output pulses seen at both P_1 and P_2 are shown in Figure 4c along with the values seen at P_3 in Figure 4d. As in the previous sections, pulses of $+/-$ polarity are identified within the red/ blue regions, respectively. The 0 V-line (the conditions for $A = B$ and C which results in no output pulse seen at P_1 and P_2) is represented by a black dashed line in the $P_1 = P_2$ plot (Figure 4c) following the path $2C = -A = -B$ and by a red dashed line in the P_3 plot (Figure 4d) following the path $C = 4A = 4B$. For completeness, the amplitudes of the output pulses seen at P_1 and P_2 when following P_3's 0 V-line and the amplitude at P_3 when following the $P_1 = P_2$'s 0 V-line are shown in the top and bottom panel of Figure 4e, respectively. As observed in the top panel of Figure 4e, when the 0 V-line condition of P_3 is met (i.e., $C = 4A$) the resulting output pulses at P_1 and P_2 have an amplitude of $3A$. This can be interpreted as the splitting of the incident pulse from P_3 evenly between P_1 and P_2, as one would expect given that all the waveguides have the same dimensions and filling materials. In this interpretation, the incident pulses from P_1 and P_2 both eliminate the signals toward P_3 and enhance the transmitted pulses to P_1 and P_2 resulting in all the power being evenly divided between P_1 and P_2. The bottom panel of Figure 4d shows that when the 0 V-line condition for P_1 (or P_2) is met, the output pulse amplitude seen at P_3 is $3A/2$.

Following this setup, let us consider the case where A and B are now free to vary while C is held at $-(1/2)$V. Note that this corresponds to an arbitrary value, as an example; a *matched* condition can be found for any value of C. The range of the possible received signals at each output port is shown in **Figure 5**. Here,

the top panels represent the range of attainable output amplitudes seen in P_1, P_2, and P_3, respectively, from left to right. As observed, the symmetry of P_1 and P_2 is now broken compared to the results shown in Figure 4, leading to them having separate 0 V-lines, namely, $B = A/2 + 1/2$, $B = 2A - 1$, and $B = -A + 1/4$ for P_1, P_2, and P_3, respectively. From these results, if one wants to eliminate the pulses traveling toward P_1 and P_2, the matching conditions for both P_1 and P_2 must be met simultaneously, as expected. This occurs at the intercept between P_1 and P_2's 0 V-lines (i.e., $A = 1$, $B = 1$), as can be seen in the bottom panels of Figure 5a,b. This is an expected result as the *matched* vector for $C = -(1/2)$V is $x = [1,1,-1/2]$V. These results demonstrate that other than the trivial case of $x = [0,0,0]$ V, the only input vectors that result in no reflection seen at P_1 and P_2 are the *matched* input vectors. This performance was verified via numerical simulations considering four different cases for the input vector x: 1) $x = [2,2,-1]$V, 2) $x = [1,3,-1]$V, 3) $x = [1,2,-1]$V, and 4) $x = [2,3,-1]$V. The numerical results for cases 1 and 2 are shown in **Figure 6**a,b, respectively. The results for cases 3 and 4 can be found in the Supporting Information for completeness. As observed, the scenario shown in Figure 6a represents the *matched* condition discussed in Figure 4a,b while the other scenarios from Figure 6b and Supporting Information represent slight deviations from this *matched* configuration. As it is shown, reflections down P_1 and P_2 are observed in all cases except for the *matched* scenario, corroborating the performance of the proposed pulse director. Moreover, note that these numerical results are in excellent agreement with the analytically calculated values found through Equation (1) where $x = [2,2,-1]$V results in $y = [0,0,3]$V, $x = [1,3,-1]$V to $y = [1, -1, 3]$V, $x = [1,2,-1]$V to $y = [1/3,-2/3,7/3]$V, and $x = [2,3,-1]$V to $y = [2/3, -1/3, 11/3]$V. In the numerical results, the vectors y are $y = [-0.0049, -0.0049, 3.0042]$, $y = [0.9984, -1.0082, 3.0042]$, $y = [0.3313, -0.6720, 2.3373]$, and $y = [0.6622, -0.3411, 3.6710]$, respectively.
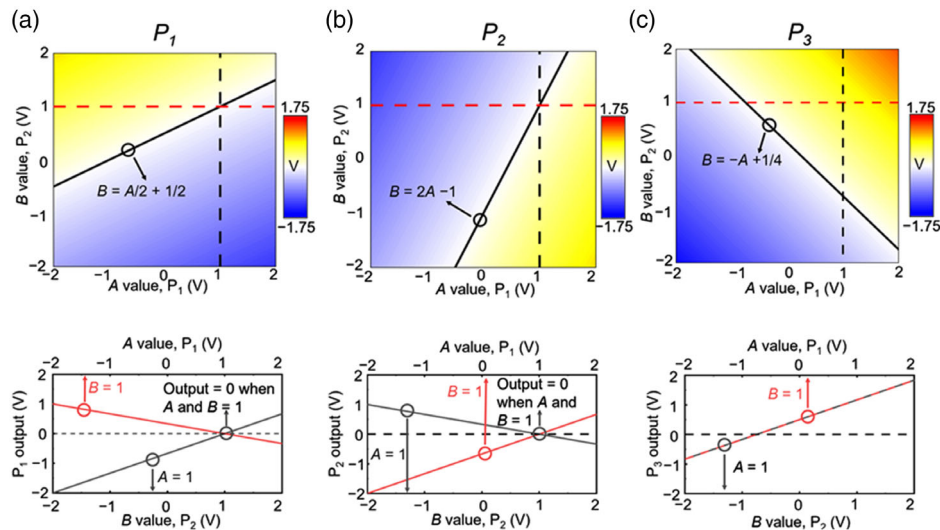

Figure 5. Three input pulse director with uneven inputs. Output pulse amplitudes of the pulse director when $A \in [-2,2]$V, $B \in [-2, 2]$V, and $C = -(1/2)$V. a–c) Show the output pulse amplitudes at P_1, P_2, and P_3, respectively. The line plots beneath each panel show the amplitude of pulses seen at P_1, P_2, and P_3 when following the black and red dashed lines shown on the contour plot above.

ADVANCED
SCIENCE NEWS
www.advancedsciencenews.com

ADVANCED
INTELLIGENT
SYSTEMS
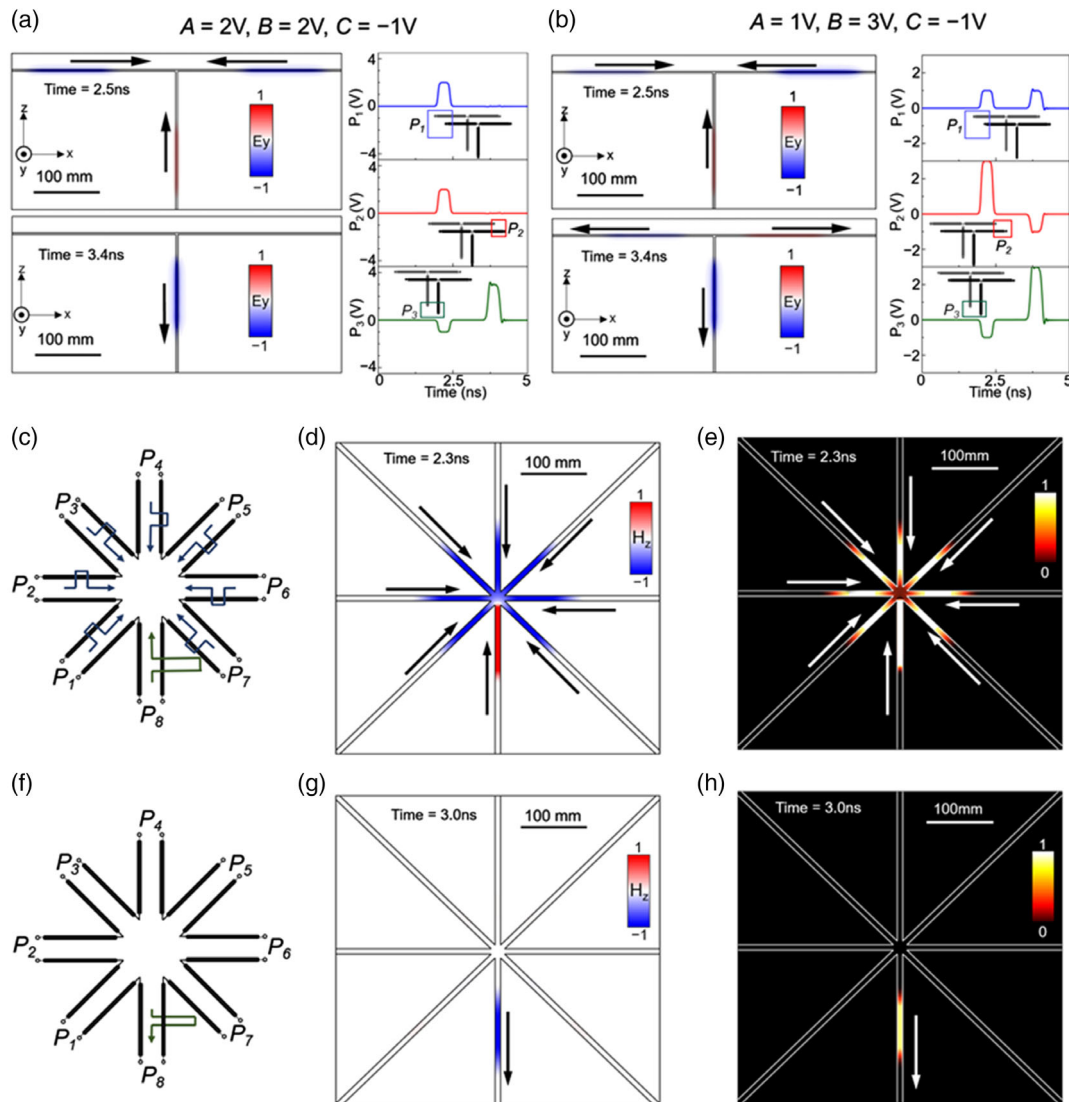Open Access
www.advintellsyst.com

Figure 6. Pulse director, numerical results. a,b) (left) Snapshots E_y field distribution at times before, $t = 2.5$ ns, and after, $t = 3.4$ ns, the incident TEM square pulses from P_1 to P_3 have passed the crossing region, respectively. All color scales for E_y are normalized to 633 V m^{-1}, corresponding to the maximum E_y field obtained from the numerical results for an incident TEM pulse of 2 V. Note that this value is close to the expected maximum when considering an ideal waveguide with infinite plate size along the transversal xy plane (666.7 V m^{-1}). The right panels in a,b) show the voltage as a function of time for all three ports. a) $A = 2$ V, $B = 2$ V, $C = -1$ V and b) $A = 1$ V, $B = 3$ V, $C = -1$ V. c,f) TL representation of an eight-waveguide series junction with ports labeled P_1 to P_8 for times before and after the pulses have passed the crossing region, respectively. d,e) Snapshot of the normalized H_z-field and power distribution, respectively, at a time ($t = 2.3$ ns) before the pulses have reached the junction. g,h) Same cases as d,e) but at a time after the junction interaction ($t = 3.0$ ns). The bottom waveguide is excited with a -3 V TEM pulse and all other are excited with a 1 V pulse. This results in a -4 V pulse in the bottom waveguide and no other pulses present. The color scales for the panels corresponding to a time before the incident TEM pulses have reached the junction ($t = 2.3$ ns, panels d) and e) are normalized to the maximum value of the out-of-plane H_z-field and power distribution values, respectively, corresponding to an input pulse of 1 V (1 A m^{-1} and 375 W m^{-2}, respectively). The color scales for the results $t = 3$ ns g,h) are normalized to 4 A m^{-1} and 6000 W m^{-2}, respectively, corresponding to the peak values for an incident pulse of -4 V.

2.4. *Pulse Director* in *N*-Interconnected Waveguides

As we mentioned in the previous section, the proposed pulse directing technique can be generalized to a *N*-waveguide junction by following the same reciprocity approach described for the three-waveguide configuration in Figure 4a,b. Whereas discussions of the comparator and the three-waveguide pulse director

in the previous sections have been applied to parallel junctions, in this section we will study the case of *N*-interconnected waveguides using series junctions (see Figure 1b). The purpose of this is twofold: 1) to show how the pulse directing technique can be applied to both series and parallel junction setups and 2) to demonstrate the extension of our technique to an arbitrary number of waveguides. As can be demonstrated in Section S1, Supporting

**ADVANCED
SCIENCE NEWS**

www.advancedsciencenews.com

**ADVANCED
INTELLIGENT
SYSTEMS**
Open Access

www.advintellsyst.com

Information, the scattering matrix for a N-waveguide series junction can be written as $A_{\text{series}} = -A_{\text{parallel}}$. This implies that any vector which is *matched* for one junction setup is also *matched* for the other as the output vector γ is simply multiplied by a factor of -1.

As described in the previous sections, for an N-input waveguide junction any single incident pulse applied from a port will result in the creation of N pulses (one per waveguide) after the incident pulse passes the junction. From Equation (1), it can be seen that for a N-waveguide series junction the transmitted (toward the nonincident ports) and reflected (toward the incident port) pulses will have an amplitude $-2/N$ and $(N - 2)/N$ multiplied by the incident pulse amplitude, respectively.[59,64] For example, considering an incident pulse with an amplitude of 1 V from the Nth waveguide, the output pulse vector is $\gamma = [-2/N, -2/N, \ldots, (N - 2)/N]$V. As before, the reciprocity of the system implies that if this vector γ is applied as an input vector, then only a single pulse in the Nth waveguide would be observed after the incident pulses pass the waveguide junction. In this context, the *matched* vector for a N-waveguide junction is thus xmatched $= [-2/N, -2/N, \ldots, (N - 2)/N]$. As any vector that can be written in the form $x = \zeta x_{\text{matched}}$ is also a *matched* vector, the above *matched* vector can be simplified into the form

$$x_{\text{matched}} = [1, 1, \ldots, (2 - N)/2] \tag{6}$$

This performance was corroborated by full wave numerical simulations using the time domain solver of the commercial software COMSOL Multiphysics (see details about the simulation setup in the Experimental Section) and the numerical results of an eight-waveguide series junction are shown in Figure 6d–h along with the TL representation of this configuration in Figure 6c,f. Here, we excite ports P_1–P_7 with a 1 V TEM square pulse and P_8 with a -3 V pulse. The input x vector of this excitation is then $x = [1,1,1,1,1,1,1,-3]$V, which corresponds to a *matched* input vector. Note that P_8 is situated at the bottom in all panels in Figure 6c–h. Figure 6c–h shows the schematic representation of the equivalent TL (Figure 6c), normalized out-of-plane H_z-field distribution (Figure 6d), and the normalized power distribution (Figure 6e) of the incident pulses at a time ($t = 2.3$ ns) before their interaction at the junction. The field distributions and TL sketch at a time ($t = 3$ ns) after the incident pulses have passed the crossing region are shown in Figure 6f–h. As observed, only one pulse is visible traveling toward P_8 with an amplitude of -3.99 V, in agreement with the theoretical values using Equation (1) which predicts an output vector $\gamma = [0,0,0,0,0,0,0,-4]$V, demonstrating how the proposed decision-making process can be implemented in N-interconnected waveguides.

As explained in this work, the comparator and pulse director devices here studied could be exploited in computing processes as they represent primitive operations. For example, for a three-waveguide junction as those evaluated in the previous sections, the existence, or lack thereof, of reflected pulses observed at P_1 and P_2 represent two distinct switching states, which in the realm of decision-making processes can be interpreted as True or False values. As previously discussed in this article, this enables elementary If...Then...Else operations to be processed with a high speed (with the velocity of light in the medium filling the waveguides). For example, if a pulse of amplitude $-(1/2)$V is excited in P_3 it is possible to emulate an AND structure between the pulses excited in P_1 and P_2. In this case, the *matched* vector will be $x = [1,1,-1/2]$V, which leads to the conditional structure: "If (Pulse amplitude in P_1) $== 1$ V AND (Pulse amplitude in P_2) $== 1$ V then Return (No reflected pulses), else Return (Reflected pulses)." In this case, "(No reflected pulses)" would be interpreted as True and "(Reflected pulses)" would be interpreted as False. The structures presented in this work may be scaled down to allow for more compact devices and shorter pulse durations. In such scenarios dispersion of the metals involved in the design should be considered,[69] as we have shown in our previous work.[57] These results demonstrate the potential of controlling the switching process of TEM square pulses in interconnected waveguide junctions. We envision that such scenarios may open new avenues in high-speed computing as decision-making processes such as If...Then...Else are key primitives in computing systems.

3. Conclusion

In this work, we have proposed and demonstrated a computing technique that exploits the splitting of TEM pulses of different amplitudes and polarities (representing the information to be processed) being excited from multiple ports and traveling within multiple waveguides connected either in a parallel or series junction configuration. The fundamental physics of TEM pulse propagation in such junctions has been presented and studied using transmission lines techniques, demonstrating how the interaction of multiple incident pulses is the result of the power division and superposition of the incident pulses within the system. To explore the opportunities of our technique for decision-making processes as fundamental for computing systems, two applications have been presented: a comparator and a pulse director, showing how they can be designed to decern the larger value between two numbers or to achieve similar performances as traditional logic gates (here emulated via an analogue linear system), respectively. Further work with these design principles may also enable more decision-making processes such as the emulation of majority logic gates and linear logic operators based on the superposition of TEM pulses. We envision that our technique may find applications in wave/pulse-based processors and could be potentially merged with electronic systems and devices (such as CMOS technologies) opening new directions for future high-speed computing systems.

4. Experimental Section

The numerical simulations shown in Figure 3 and 6 were performed using the transient solver of the commercial software CST studio suite. Perfect electric conductor (PEC) was used for the metallic plates having a zero thickness. All the waveguides were designed with parallel plates having a transversal dimension of 3 mm (width) and a length of 250 mm to the center of the junction. For the three interconnected waveguides in parallel, the distance between the plates was 3 mm. Vacuum ($\varepsilon_r = 1$, $\mu_r = 1$) was used as both the filling material of the waveguides and the background medium. Waveguide ports were used to excite the waveguides with pulses of different polarities and amplitudes having a duration of 0.4 ns in their nonzero state. For the parallel plate

**ADVANCED
SCIENCE NEWS**

www.advancedsciencenews.com

**ADVANCED
INTELLIGENT
SYSTEMS**
Open Access

www.advintellsyst.com

configurations in Figure 3 and 6, top and bottom "open-(add space)" boundary condition was implemented to numerically evaluate the performance of the junctions when they are immersed within an infinite vacuum background. The rest of the boundaries were simulated with an "Open" boundary condition. The numerical simulations for the N-waveguide series junction shown in Figure 6 were carried out using the time-domain solver of the commercial software COMSOL Multiphysics using the same materials as in the results discussed in Figure 3 and 6. In this case, a distance of 10 mm between the plates was considered. Scattering boundary conditions were used at the entrance of each waveguide to both excite each of them with an incident square pulse (duration of 0.4 ns and fall/rise time of 0.08 ns with a second derivative smoothing) and to absorb the pulses traveling toward the waveguides after the incident pulses have passed the crossing region.

Supporting Information

Supporting Information is available from the Wiley Online Library or from the author.

Conflict of Interest

The authors declare no conflict of interest.

Author Contributions

V.P.-P. and A.Y.: conceived the original idea of using interconnected transmission lines for switching of multiple TEM pulses with different amplitudes; R.G.M.: conducted the numerical simulations and analytical calculations; All the authors were involved in the discussion and interpretation of the results; R.G.M.: wrote the first draft of the article and then V.P.-P and A.Y. commented, edited, and worked on the subsequent drafts of the article; V.P.-P.: supervised the project.

Data Availability Statement

The data that support the findings of this study are available from the corresponding author upon reasonable request.

[1] G. E. Moore, *Proc. IEEE* **1998**, *86*, 82.

[2] J. Mardinly, *Micros. Today* **2007**, *15*, 6.

[3] C. P. Yue, S. S. Wong, in *2005 IEEE Radio Frequency integrated Circuits*, IEEE, Piscataway, NJ **2005**, pp. 53–56, https://doi.org/10.1109/RFIC.2005.1489494.

[4] F. Adamu-Lema, *The scaling of MOSFETs, Moore's law, and ITRS in Scaling and intrinsic parameter fluctuations in nano-CMOS devices, Ph.D thesis*, University of Glasgow, Glasgow **2005**.

[5] G. Mcfarland, M. Flynn, *Limits of scaling MOSFETS, Technical Report CSL-TR-95-62*, Stanford University, California, USA **1995**.

[6] J. M. Shalf, R. Leland, *Computer* **2015**, *48*, 14.

[7] R. S. Williams, *Comput. Sci. Eng.* **2017**, *19*, 7.

[8] T. N. Theis, H.-S. P. Wong, *Comput. Sci. Eng.* **2017**, *19*, 41.

[9] I. L. Markov, *Nature* **2014**, *512*, 147.

[10] A. Hirohata, K. Yamada, Y. Nakatani, P. Ioan-Lucian, B. Diény, P. Pirro, B. Hillebrands, *J. Magn. Magn. Mater.* **2020**, *509*, 166711.

[11] Y. Benenson, *Nat. Rev. Genet.* **2012**, *13*, 455.

[12] D. Woods, T. J. Naughton, *Appl. Math. Comput.* **2009**, *215*, 1417.

[13] M. A. Habli, *Opt. Eng.* **1993**, *32*, 642.

[14] M. N. Islam, C. E. Soccolich, D. A. B. Miller, *Opt. Lett.* **1990**, *15*, 909.

[15] F. Reynaud, A. Barthelemy, in *AND Optical Gate Using Soliton-Beams Interaction, Proc. SPIE 1319, Optics in Complex Systems*, July **1990**, https://doi.org/10.1117/12.22205.

[16] M. N. Islam, *Opt. Lett.* **1989**, *14*, 1257.

[17] M. N. Islam, C. E. Soccolich, J. P. Gordon, *Opt. Quantum Electron.* **1992**, *24*, S1215.

[18] A. Ghadi, S. Sohrabfar, *IEEE Photonics Technol. Lett.* **2018**, *30*, 569.

[19] F. Zangeneh-Nejad, R. Fleury, *New J. Phys.* **2018**, *20*, 073001.

[20] F. Zangeneh-Nejad, R. Fleury, *Nat. Commun.* **2019**, *10*, 2058.

[21] A. Silva, M. Francesco, C. Giseppe, G. Vincenzo, A. Andrea, E. Nader, *Science* **2014**, *343*, 160.

[22] V. Fedotov, in *Springer Handbook of Electronic and Photonic Materials, Springer Handbooks* (Ed: S. Kasap, P. Capper), Springer, Cham **2017**, https://doi.org/10.1007/978-3-319-48933-9_56.

[23] Q. Zhao, J. Zhou, F. Zhang, D. Lippens, *Mater. Today* **2009**, *12*, 60.

[24] C. Della Giovampaola, N. Engheta, *Nat. Mater.* **2014**, *13*, 1115.

[25] T. Chen, S. Li, H. Sun, *Sensors* **2012**, *12*, 2742.

[26] Y. Lee, S.-J. Kim, H. Park, B. Lee, *Sensors* **2017**, *17*, 1726.

[27] Y. Dong, T. Itoh, *Proc. IEEE* **2012**, *100*, 2271.

[28] S. Naoui, L. Latrach, A. Gharsallah, *Microw. Opt. Technol. Lett.* **2014**, *56*, 2899.

[29] C. Jouvaud, A. Ourir, J. de Rosny, *Appl. Phys. Lett.* **2014**, *104*, 243507.

[30] N. Kundtz, D. R. Smith, *Nat. Mater.* **2010**, *9*, 129.

[31] V. Pacheco-Peña, N. Engheta, *Light Sci. Appl.* **2020**, *9*, 129.

[32] V. Pacheco-Peña, N. Engheta, *Nanophotonics* **2020**, *9*, 379.

[33] V. Pacheco-Peña, N. Engheta, *Optica* **2020**, *7*, 323.

[34] V. Pacheco-Peña, N. Engheta, *Phys. Rev. B* **2021**, *104*, 214308.

[35] C. Caloz, Z.-L. Deck-Léger, *IEEE Trans. Antennas Propag.* **2019**, *68*, 1569.

[36] L. Quan, S. Yves, Y. Peng, H. Esfahlani, A. Alù, *Nat. Commun.* **2021**, *12*, 2615.

[37] A. N. Z. Rashed, A. E.-N. A. Mohammed, W. F. Zaky, I. Amiri, P. Yupapin, *Results Phys.* **2019**, *13*, 102152.

[38] N. Mohammadi Estakhri, B. Edwards, N. Engheta, *Science* **2019**, *363*, 1333.

[39] T. Zhu, Y. Zhou, Y. Lou, H. Ye, M. Qiu, Z. Ruan, S. Fan, *Nat. Commun.* **2017**, *8*, 15391.

[40] A. Pors, M. G. Nielsen, S. I. Bozhevolnyi, *Nano Lett.* **2015**, *15*, 791.

[41] S. Abdollahramezani, O. Hemmatyar, A. Adibi, *Nanophotonics* **2020**, *9*, 4075.

[42] A. Momeni, K. Rouhi, R. Fleury, *Carbon* **2022**, *186*, 599.

[43] F. Zangeneh-Nejad, D. L. Sounas, A. Alù, R. Fleury, *Nat. Rev. Mater.* **2021**, *6*, 207.

[44] H. Goh, A. Alù, *Phys. Rev. Lett.* **2022**, *128*, 073201.

[45] J. L. O'Brien, *Science* **2007**, *318*, 1567.

[46] T. D. Ladd, F. Jelezko, R. Laflamme, Y. Nakamura, C. Monroe, J. L. O'Brien, *Nature* **2010**, *464*, 45.

[47] E. Feigenbaum, M. Orenstein, *Opt. Express* **2007**, *15*, 17948.

[48] E. Feigenbaum, H. A. Atwater, *Phys. Rev. Lett.* **2010**, *104*, 147402.

[49] M. Gaio, D. Saxena, J. Bertolotti, D. Pisignano, A. Camposeo, R. A. Sapienza, *Nat. Commun.* **2019**, *10*, 226.

[50] K. Wu, C. Soci, P. P. Shum, N. I. Zheludev, *Opt. Express* **2014**, *22*, 295.

[51] S. Dutta, O. Zografos, S. Gurunarayanan, I. Radu, B. Soree, F. Catthoor, A. Naeemi, *Sci. Rep.* **2017**, *7*, 17866.

[52] P. Sharma, V. D. Kumar, *IEEE Photonics Technol. Lett.* **2018**, *30*, 959.

[53] T. Birr, U. Zywietz, P. Chhantyal, B. N. Chichkov, C. Reinhardt, *Opt. Express* **2015**, *23*, 31755.

[54] Y. Fu, X. Hu, C. Lu, S. Yue, H. Yang, Q. Gong, *Nano Lett.* **2012**, *12*, 5784.

[55] J. Xie, X. Niu, X. Hu, F. Wang, Z. Chai, H. Yang, Q. Gong, *Nanophotonics* **2017**, *6*, 1161.

[56] S. Asgari, N. Granpayeh, Z. G. Kashani, *IEEE Trans. Nanotechnol.* **2019**, *18*, 42.

[57] S. Siccardi, A. Adamatzky, *Int. J. Bifurcation Chaos* **2016**, *26*, 1650107.

[58] S. Siccardi, J. A. Tuszynski, A. Adamatzky, *Phys. Lett. A* **2016**, *380*, 88.

[59] A. Yakovlev, V. Pacheco-Peña, *Adv. Mater. Technol.* **2020**, *5*, 2000796.

[60] A. Ventisei, A. Yakovlev, V. Pacheco-Peña, *Adv. Theory Simul.* **2021**, *2100429*, 2100429.

[61] C. Christopoulos, *Synth. Lect. Comput. Electromagn.* **2006**, *1*, 1.

[62] I. Catt, *Electromagnetics 1*, Westfields Press, St Albans, UK **1995**.

[63] L. Qian, H. J. Caulfield, *Inf. Sci. Int. J.* **2006**, *176*, 3379.

[64] D. M. Pozar, *Microwave Engineering*, John wiley & sons, Hoboken, New Jersey **2011**.

[65] K. Hoffmann, Z. Skvor, *IEEE Trans. Microw. Theory Tech.* **1998**, *46*, 2520.

[66] D. F. Williams, J. C. M. Wang, U. Arz, *IEEE Trans. Microw. Theory Tech.* **2003**, *51*, 2391.

[67] V. Pacheco-Peña, A. Yakovlev, in *Handbook of Unconventional Computing* (Ed: A. Adamatzky), World Scientific, London, UK **2021**, pp. 465–492, https://doi.org/10.1142/9789811235740_0016.

[68] C. E. Shannon, *Trans. Am. Inst. Electr. Eng.* **1938**, *57*, 713.

[69] E. Silaeva, L. Saddier, J.-P. Colombier, *Appl. Sci.* **2021**, *11*, 9902.

2200137 (11 of 11)